



JOURNAL OF
APPLIED
CRYSTALLOGRAPHY

Volume 49 (2016)

Supporting information for article:

Versatile electrochemical cell for Li-/Na-ion batteries and high-throughput setup for combined *operando* X-ray diffraction and absorption spectroscopy

Jonas Sottmann, Roberto Homs-Regojo, David S. Wragg, Helmer Fjellvåg, Serena Margadonna and Hermann Emerich

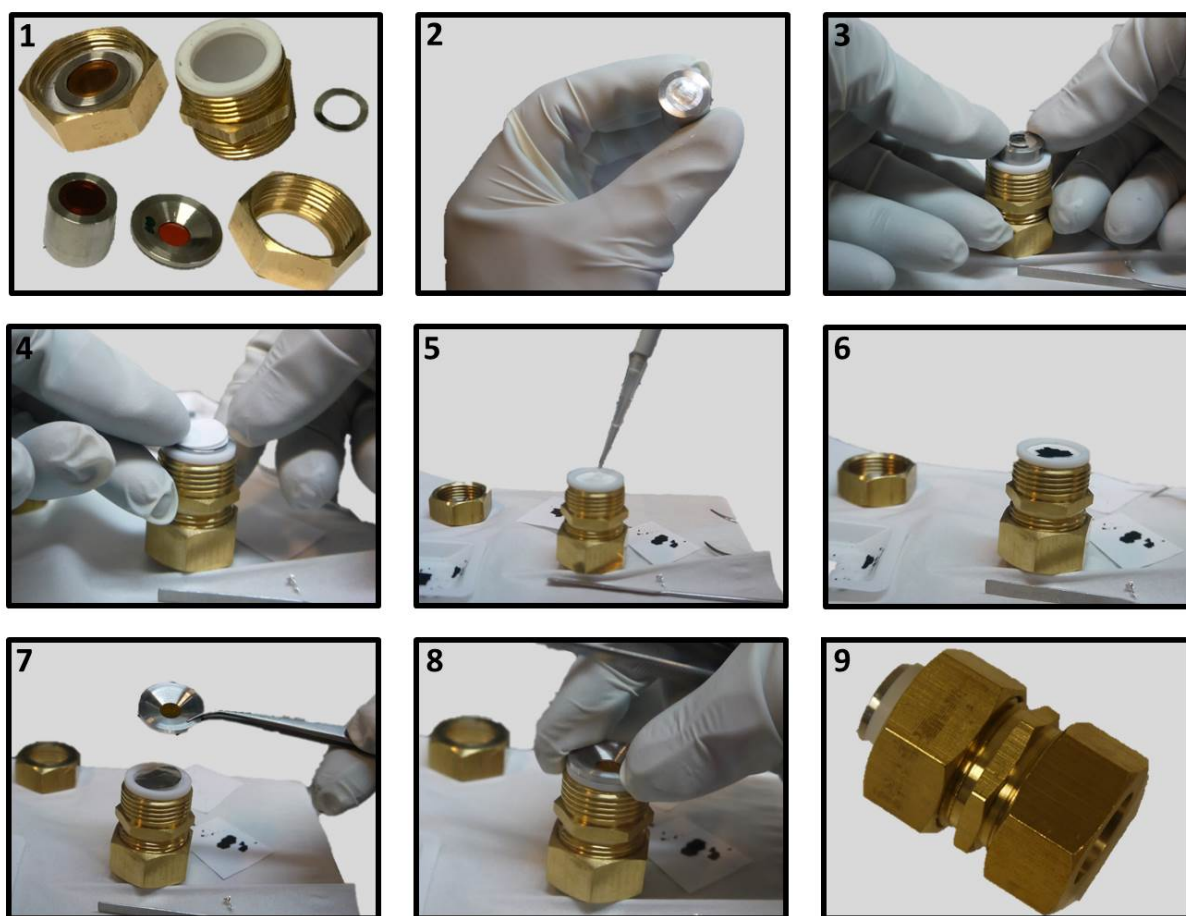


Figure S1 Assembly procedure: (1) Various parts of the cell shown in the assembling order; piston **C**, Teflon cylinder **T**, spring, piston **B**, battery as show in (2) to (7) and finally piston **A**; (2) Na or Li metal spread on piston **B**; (3) piston **B** placed in Teflon cylinder **T** on top of piston **C** and a spring; (4) glass fiber separator; (5) electrolyte; (6) self-standing electrode; (7) metal foil (or electrode coated on metal foil); (8) piston **A**; (9) closed cell.

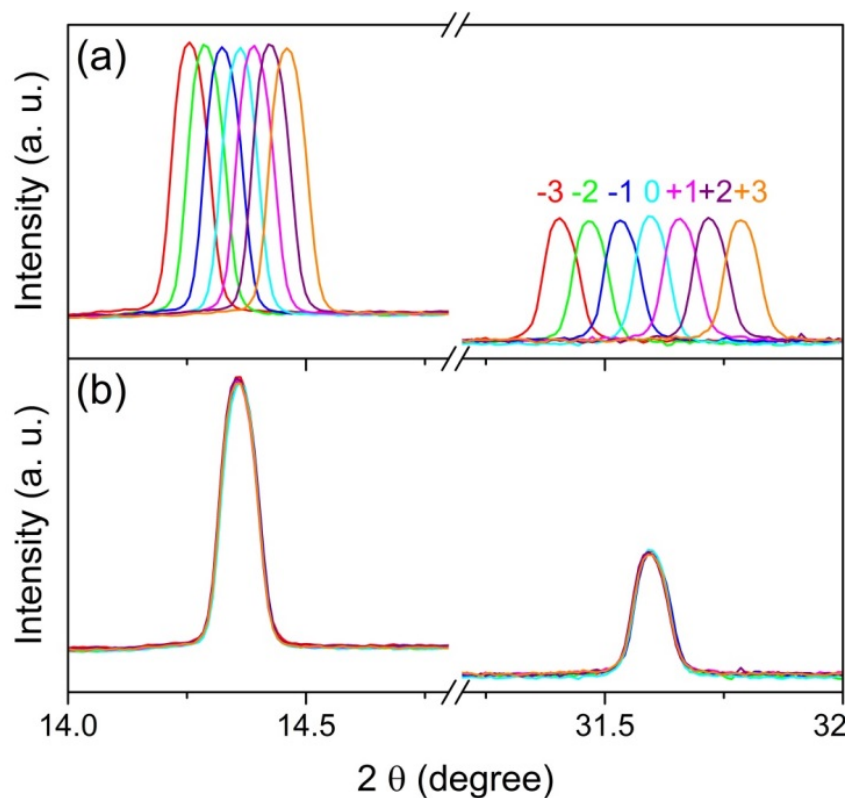


Figure S2 (a) Diffraction profiles ($\lambda = 0.50648 \text{ \AA}$) of Al foil in a cell mounted in the center of the diffractometer (zero position) and displaced in 1 mm steps in the range of ± 3 mm from the center and (b) corrected for the displacement error prior to data reduction with pyFAI (Ashiotis *et al.*, 2015). For this purpose the distance parameter was modified iteratively in pyFAI (here by -3, -2, -1, +1, +2 and +3 mm) until the Al peak of the cell in zero and displaced positions matched.

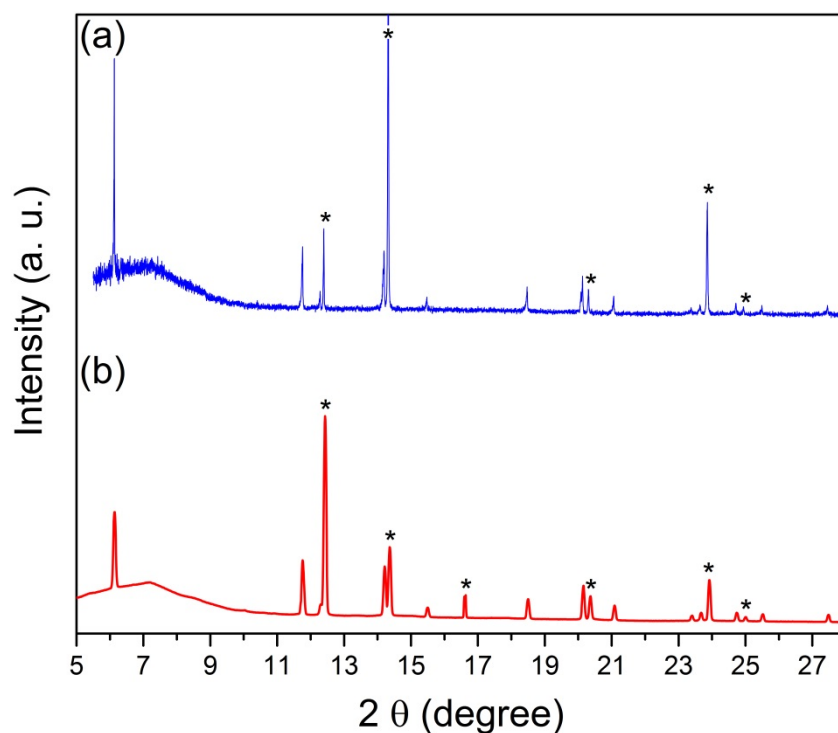


Figure S3 Diffraction profiles ($\lambda = 0.50480 \text{ \AA}$) of a pristine SNBL cell loaded with $\text{LiMn}_{1.5}\text{Ni}_{0.5}\text{O}_4$ using (a) the 1D high resolution powder diffractometer with 6 Si-111 analyzer and (b) the Dexela 2923 CMOS 2D detector (Abdala *et al.*, 2014) with high counting statistics at the SNBL. The Bragg peaks marked with an asterisk are from the metallic Li in the cell, different relative intensities for corresponding peaks in the different patterns are due to texture in the Li foil which is observed as “spotty” diffraction patterns in the 2D images (Herklotz *et al.*, 2013).

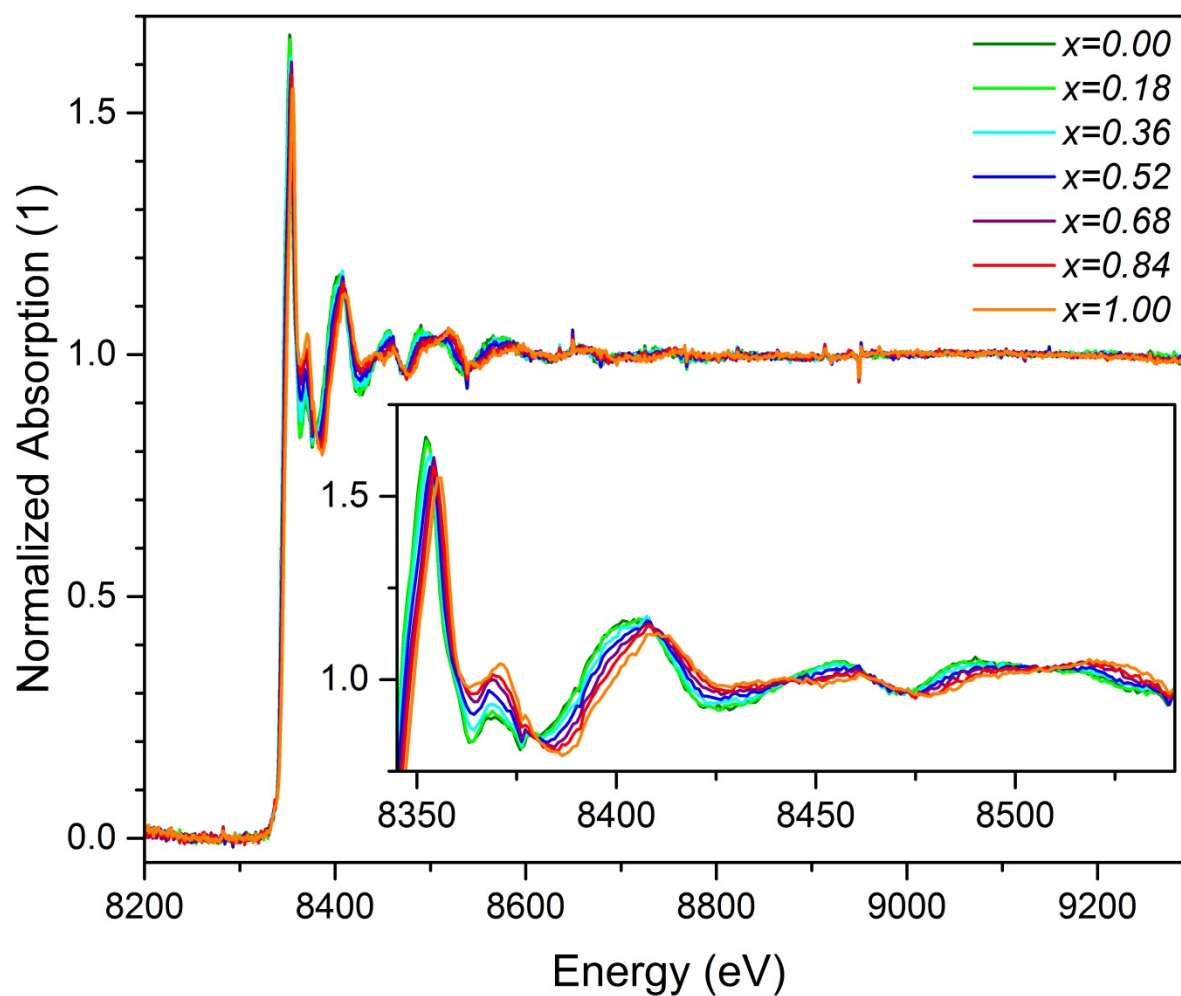


Figure S4 Normalized EXAFS spectra of $\text{Li}_{1-x}\text{Mn}_{1.5}\text{Ni}_{0.5}\text{O}_4$ as a function of x .

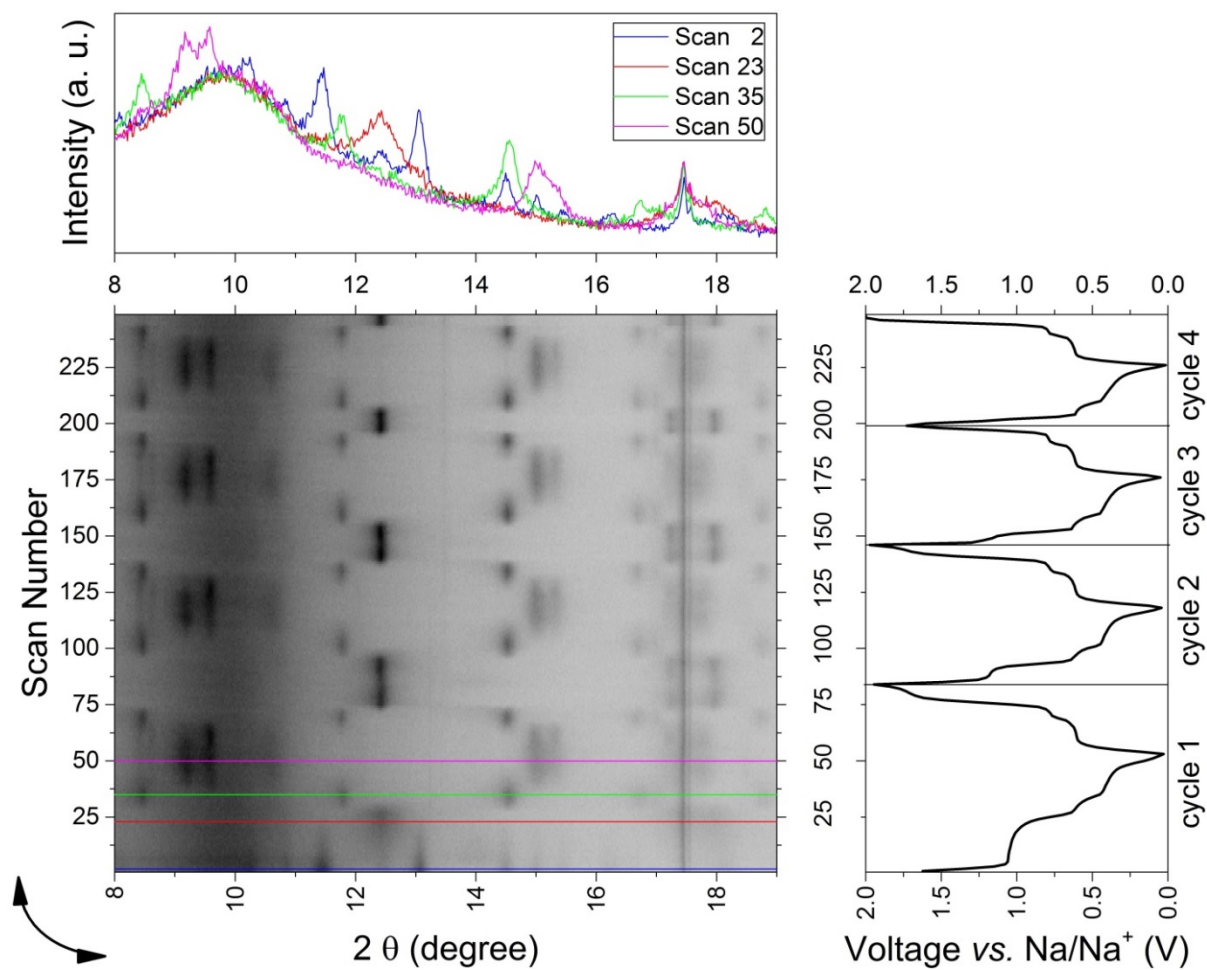


Figure S5 Operando XRD data collected Bi_2S_3 as SIB anode using a Bruker D8 with Mo source in transmission mode Bi_2S_3 . The dark color in the film plots corresponds to high intensities.

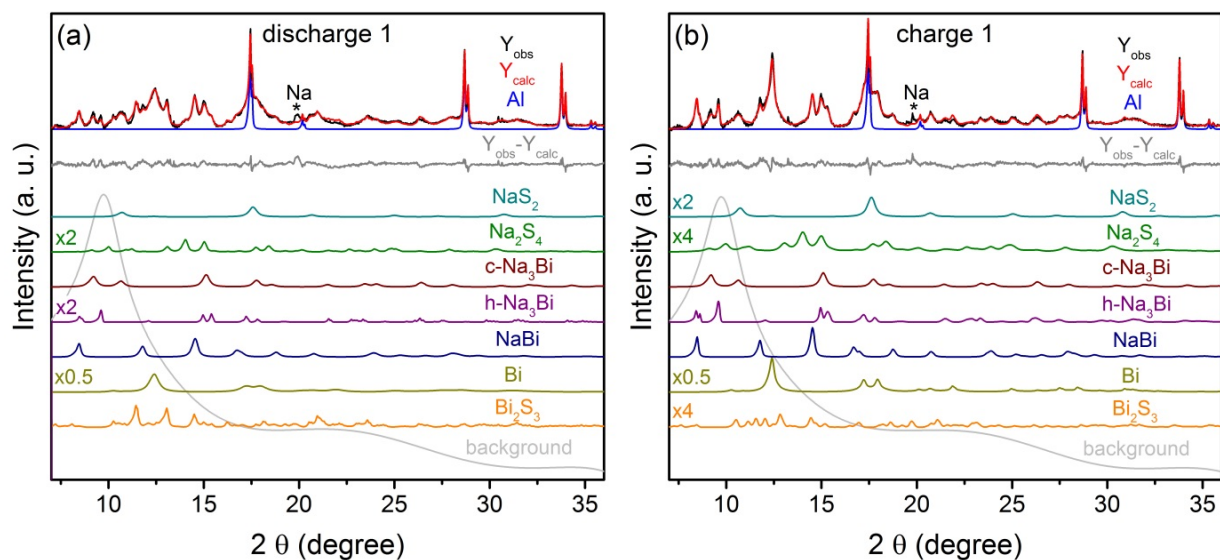


Figure S6 Summed intensities of all powder patterns collected during the first charge (a) and discharge (b), respectively, vs. calculated intensity and deconvoluted contributions from all phases to the calculated intensity. The background is represented as the light gray line.

Table S1 Crystallographic details of the Na-Bi-S system.

phase	space group, structure	a (Å)	b (Å)	c (Å)	crystallite	
					size 1 (nm)	size 2 (nm)
Bi ₂ S ₃	<i>Pbnm</i> (62), Sb ₂ S ₃	11.15	11.27	3.98	3	56
Bi	<i>R-3m</i> (166), As	4.54	a	11.84	4	23
NaBi	<i>P4/mmm</i> (123), AuCu	3.45	a	4.79	3	21
h-Na ₃ Bi	<i>P6₃/mmc</i> (194), Na ₃ As	5.44	a	9.65	-	63
c-Na ₃ Bi	<i>Fm-3m</i> (225), Li ₃ Bi	7.65	a	a	-	63
Na ₂ S ₄	<i>I-42d</i> (122), Na ₂ S ₄	9.55	a	11.73	4	-
Na ₂ S	<i>Fm-3m</i> (225), Fluorite-CaF ₂	6.58	a	a	4	-

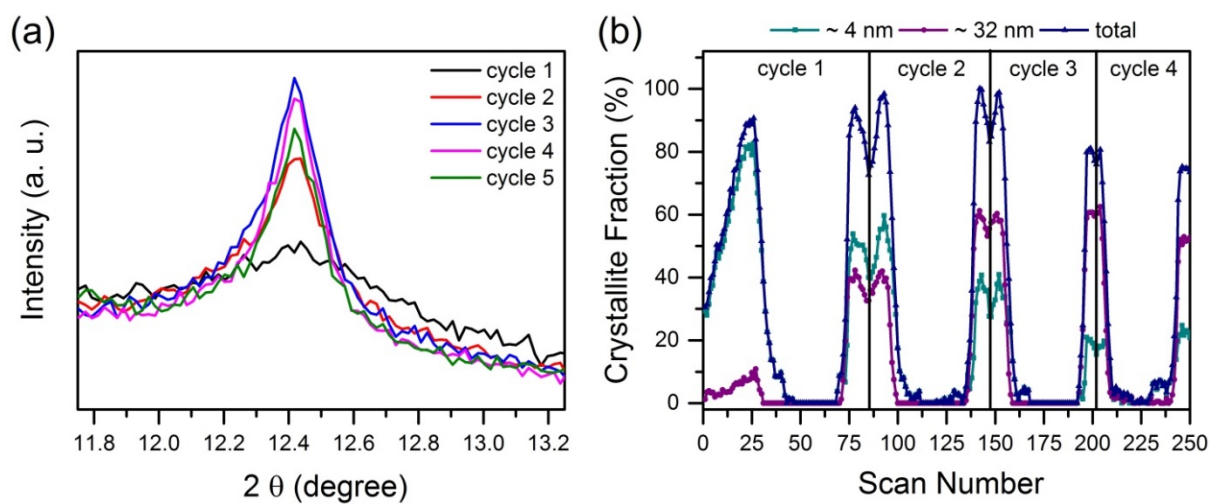


Figure S7 Bi (0 1 2) peak broadening vs. cycle number (Mo radiation). Evolution of the crystallite size distribution during the first 4 cycles.